JACS
JOURNAL OF THE AMERICAN CHEMICAL SOCIETY
Article
pubs.acs.org/JACS

Single Samarium Atoms in Large Fullerene Cages. Characterization of Two Isomers of Sm@C_{92} and Four Isomers of Sm@C_{94} with the X-ray Crystallographic Identification of Sm@C_1(42)-C_{92}, Sm@C_s(24)-C_{92}, and Sm@C_{3v}(134)-C_{94}

Hongxiao Jin,[†] Hua Yang,*[,†] Meilan Yu,[‡] Ziyang Liu,*[,‡,†] Christine M. Beavers,[§] Marilyn M. Olmstead,*[,∥] and Alan L. Balch*[,∥]

[†]College of Materials Science and Engineering, China Jiliang University, Hangzhou 310018, China
[‡]College of Life Science, Zhejiang Sci-Tech University, Hangzhou 310018, China
[§] Advanced Light Source, Lawrence Berkeley National Lab, One Cyclotron Road, Berkeley, California 94720, United States
[∥]Department of Chemistry, University of California, One Shields Avenue, Davis, California 95616, United States

Supporting Information

ABSTRACT: Two isomers of Sm@C_{92} and four isomers of Sm@C_{94} were isolated from carbon soot obtained by electric arc vaporization of carbon rods doped with Sm_2O_3. Analysis of the structures by single-crystal X-ray diffraction on cocrystals formed with Ni^{II}(octaethylporphyrin) reveals the identities of two of the Sm@C_{92} isomers: Sm@C_{92}(I), which is the more abundant isomer, is Sm@C_1(42)-C_{92}, and Sm@C_{92}(II) is Sm@C_s(24)-C_{92}. The structure of the most abundant form of the four isomers of Sm@C_{94}, Sm@C_{94}(I), is Sm@C_{3v}(134)-C_{94}, which utilizes the same cage isomer as the previously known Ca@C_{3v}(134)-C_{94} and Tm@C_{3v}(134)-C_{94}. All of the structurally characterized isomers obey the isolated pentagon rule. While the four Sm@C_{90} and five isomers of Sm@C_{84} belong to common isomerization maps that allow these isomers to be interconverted through Stone–Wales transformations, Sm@C_1(42)-C_{92} and Sm@C_s(24)-C_{92} are not related to each other by any set of Stone–Wales transformations. UV–vis–NIR spectroscopy and computational studies indicate that Sm@C_1(42)-C_{92} is more stable than Sm@C_s(24)-C_{92} but possesses a smaller HOMO–LUMO gap. While the electronic structures of these endohedrals can be formally described as $Sm^{2+}@C_{2n}^{2-}$, the net charge transferred to the cage is less than two due to some back-donation of electrons from π orbitals of the cage to the metal ion.

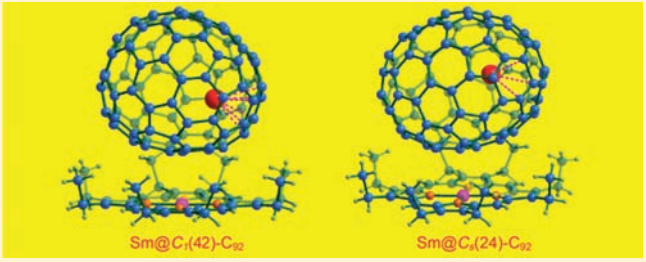

INTRODUCTION

The fullerene C_{60} has become an iconic molecule, in part because of its appealing icosahedral symmetry and similarity to a soccer ball.[1,2] Immediately following its initial detection, chemists have been interested in determining whether the inside of such a nearly spherical molecule could host other atoms or molecules. In pursuit of that idea, La@C_{60} and La_2@C_{60} were observed by mass spectrometry shortly after C_{60} was initially detected.[3] In the intervening years, many endohedral fullerenes with an array of different atoms in the interior and a variety of carbon cage sizes have been made and identified.[4−7] Some notable examples include $Sc_3N@I_h$-C_{80}, the third most abundant fullerene;[8] $Sm_2@D_{3d}$(822)-C_{104}, the largest fullerene cage to be characterized by X-ray crystallography;[9] $(H_2)_2@C_{70}$, a fullerene cage encapsulating two dihydrogen molecules;[10] and $Sc_4(\mu\text{-}O)_3@I_h$-C_{80}, a fulllerene containing a seven-atom cluster that is unknown outside this carbon cage.[11]

The simplest of the endohedral fullerenes are those containing only a single atom. A surprising array of single atoms have been found or placed inside fullerene cages including chemically inert noble gas atoms;[12] highly reactive nitrogen atoms, which do not bond to the inside of the carbon cage;[13−15] and electropositive metal atoms. When electropositive metal atoms are trapped inside carbon cages, electrons are transferred from the metal to the cage, so that an electronic structure, $M^{+x}@(C_{2n})^{-x}$, results.[16−18] Thus, for the lanthanide metals, Sc, Y, La, Ce, Pr, Nd, Gd, Tb, Dy, Ho, Er, and Lu, three electrons are transferred to the cage, and the metals adapt their usual +3 oxidation state. On the other hand, for endohedral fullerenes with alkaline earth elements or some lanthanide elements (Sm, Eu, Tm, and Yb,) only two electrons are transferred to the cage. The physical properties of these endohedral fullerenes depend upon the particular metal encapsulated. For example, endohedrals containing radioactive metals may be useful as imaging agents and in nuclear medicine.[19,20] When paramagnetic ions such as Gd^{3+} are involved, the endohedral fullerenes have magnetic properties

Received: March 23, 2012
Published: April 26, 2012

   dx.doi.org/10.1021/ja302859r | J. Am. Chem. Soc. 2012, 134, 10933−10941

that make them useful as relaxation agents in magnetic resonance imaging (MRI).[21,22]

More than 25 endohedral fullerenes containing a single samarium atom have been isolated.[23−25] These endohedral molecules involve cage sizes ranging from C_{74} to C_{96}. Electron energy-loss spectroscopic (EELS) measurements have shown that the oxidation state of the samarium is +2 in a number of these molecules.[26,27] To provide further fundamental structural information about the individual Sm@C_{2n} molecules, we have been engaged in the isolation of these endohedrals so that single-crystal X-ray diffraction data can be used to determine their structures.

To date, structural studies of endohedral fullerenes containing one samarium atom have provided the following information. Four isomers of Sm@C_{90} have been identified and isolated in sufficient quantity to determine their structures through X-ray crystallography.[28] These isomers have been identified as Sm@C_2(40)-C_{90}, Sm@C_2(42)-C_{90}, Sm@C_{2v}(46)-C_{90}, and Sm@C_2(45)-C_{90}, and constitute the most extensive series of endohedral fullerene isomers to be examined by X-ray diffraction. These four isomers can be related to each other pairwise, through a sequence of Stone−Wales transformations.[29] Scheme 1 shows the Stone−Wales transformation and

Scheme 1. Stone−Wales Transformation and the Pairwise Interconversions of the Four Isolated Sm@C_{90} Isomers

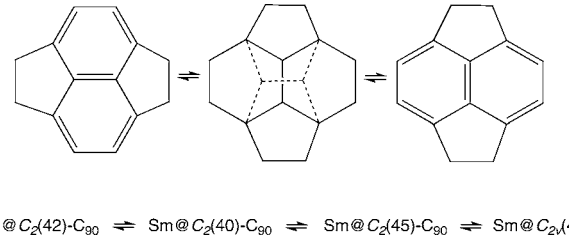

the pairwise possible transformations among four isomers Sm@C_{90}. The isomerization between two isomers of C_{78}, which are related by Stone−Wales transformations, has been experimentally observed at a temperature of ca. 1050 °C.[30] In addition, three different studies of Sm@C_{84} have produced evidence for five different isomers of this endohedral.[25,31,32] The relative abundances of these isomers appear to depend upon the chemical source of samarium used in the fullerene generation. X-ray crystallographic characterization has identified two of these isomers as Sm@D_{3d}(19)-C_{84} and Sm@C_2(13)-C_{84}.[31] On the basis of UV/vis/NIR spectral similarities to ytterbium endohedral fullerenes,[33] whose structures have been determined by ^{13}C NMR spectroscopy, two other isomers of Sm@C_{84} have been identified as Sm@C_1(12)-C_{84} and Sm@C_2(11)-C_{84}. The structure of the fifth Sm@C_{84} isomer remains unknown. Sm@C_2(13)-C_{84} and Sm@C_1(12)-C_{84} can be interconverted by a single Stones−Wales transformation, as can Sm@C_1(12)-C_{84} and Sm@C_2(11)-C_{84}. Sm@D_{3d}(19)-C_{84} cannot be converted into any of the other known Sm@C_{84} isomers by a single Stone−Wales transformation, but it can be related to these other isomers through a series of transformations involving as yet unobserved isomers.

Here, we report structural studies on some of the largest known Sm@C_{2n} endohedrals: Sm@C_{92} and Sm@C_{94}. For fullerenes larger than C_{70}, the cage can exist in different isomeric forms. The number of these isomers increases as the number of carbon atoms in the fullerene increases.[34] Thus, for C_{92} there are 86 fullerene isomers that obey the isolated pentagon rule (IPR), which requires that each pentagon be surrounded by five hexagons. If the IPR is violated, which happens for the single-atom endohedral, La@C_2-C_{72},[35] and a number of other endohedral fullerenes,[36−41] then there are 126 409 possible isomers. For C_{94}, there are 134 IPR-obeying isomers and 153 493 fullerene isomers that do not obey the IPR, but consist of a network of hexagons and 12 pentagons.

There have been only a few structural studies of fullerenes containing cage sizes as large as C_{92} and C_{94}. Two endohedral fullerenes containing a C_{92} cage have been crystallographically characterized: Gd_2C_2@D_3(85)-C_{92}[42] and Sm_2@D_3(85)-C_{92}.[43] A crystallographic study of $C_{92}(CF_3)_{16}$ formed by treatment of a mixture of higher fullerenes with trifluoromethyl iodide revealed that the D_2(82)-C_{92} isomer was a component of the mixture.[44] This process also formed $C_{94}(CF_3)_{20}$, which was characterized crystallographically and found to utilize the C_2(61)-C_{94} cage.[45] Crystallographic studies of Tm@C_{94} and the most abundant isomer of Ca@C_{94} revealed that both endohedrals use the same C_{3v}-C_{94} cage.[46]

RESULTS

Isolation of Two Isomers of Sm@C_{92}. As was outlined previously, carbon soot containing a mixture of empty cage fullerenes and samarium endohedral fullerenes was prepared by vaporizing a graphite rod filled with Sm_2O_3 and graphite powder in an electric arc.[17,28,47] The carbon soot was extracted with *o*-dichlorobenzene and concentrated. The soluble extract was then subjected to a multistage high pressure liquid chromatographic (HPLC) isolation process involving two complementary chromatographic columns (Buckyprep-M and Buckyprep) with either chlorobenzene or toluene as the eluent. Two isomers of Sm@C_{92} were isolated in relative yields of 50:3 for Sm@C_{92}(I) and Sm@C_{92}(II). Figure 1 shows the HPLC

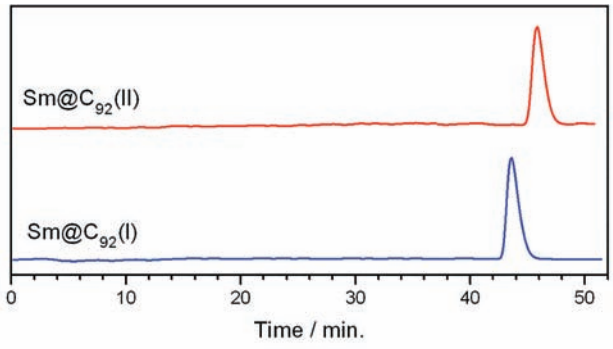

Figure 1. Chromatograms of the purified Sm@C_{92} isomers on a Buckyprep column with toluene as the eluent. The HPLC conditions are flow rate 4.0 mL/min, detecting wavelength of 450 nm.

chromatograms of the purified samples of these two Sm@C_{92} isomers. Figure 2 shows the laser-desorption, time-of-flight (LD-TOF) mass spectra of Sm@C_{92}(I) and Sm@C_{92}(II). The insets show expansion of the experimental and computed spectra.

The UV−vis−NIR absorption spectra of Sm@C_{92}(I) and Sm@C_{92}(II) are shown in Figure 3. Sm@C_{92}(I) has the lower energy onset of absorption at ca. 1330 nm and absorption bands at 1113, 979, 681, 645, and 451 nm, while Sm@C_{92}(II) displays bands at 950, 840, 682, 607, and 480 nm and an onset of absorption at ca. 1290 nm. Previously, Liu and co-workers

dx.doi.org/10.1021/ja302859r | J. Am. Chem. Soc. 2012, 134, 10933−10941

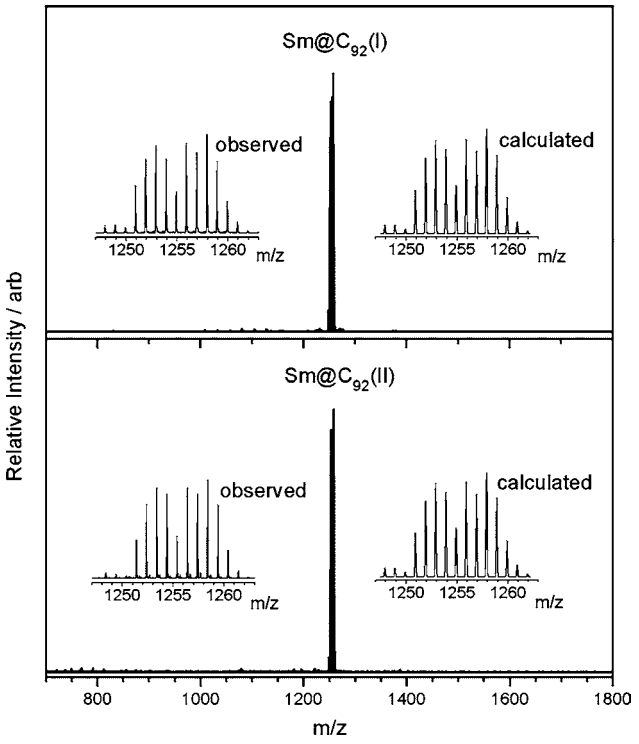

Figure 2. The LDI-TOF mass spectra of the purified samples of Sm@C_{92}(I) and Sm@C_{92}(II). The insets show expansions of the observed and calculated isotope distributions.

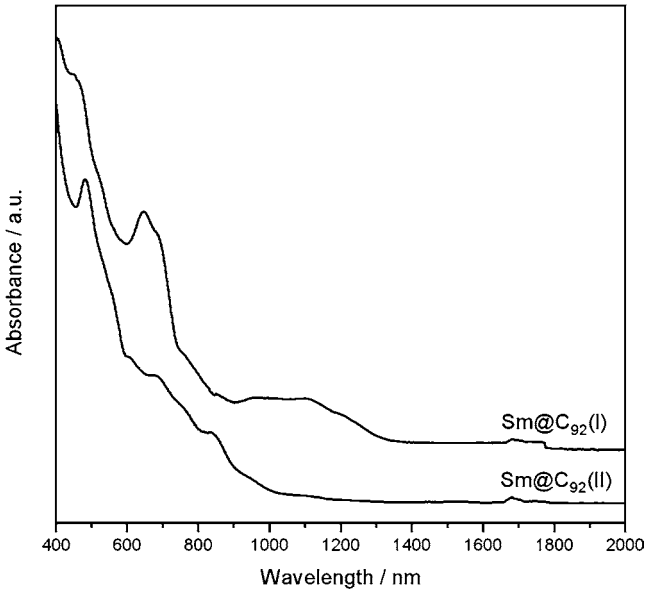

Figure 3. UV/vis/NIR absorption spectra of the purified isomers of Sm@C_{92} in carbon disulfide solution. The minor features in the 1650–1800 nm region are artifacts.

reported the isolation of two isomers of Sm@C_{92}.[25] The spectrum they report for their isomer I appears to be produced by a mixture of the two isomers reported here, whereas the spectrum they found for their isomer II corresponds to the spectrum we observed for our Sm@C_{92}(I). The spectrum of Sm@C_{92}(I) is similar to those of Yb@C_{92}[48] and Ca@C_{92},[49] but quite different from those of Gd_2C_2@D_3(85)-C_{92},[43] Dy_2C_{92}(I, II, III),[50] Er_2C_{92}(I, II, III, IV),[51,52] and La_3N@C_{92},[53] as well as that of the hollow isomer of C_{92} prepared by arc burning or combustion.[54,55]

Crystallographic Characterization of Sm@C_{92}(I) as Sm@C_1(42)-C_{92}. A sample of Sm@C_{92}(I) was cocrystallized with Ni(OEP) to facilitate crystal growth and the formation of material with sufficient internal order to allow structural analysis, as previously described.[56] Figure 4A shows a drawing

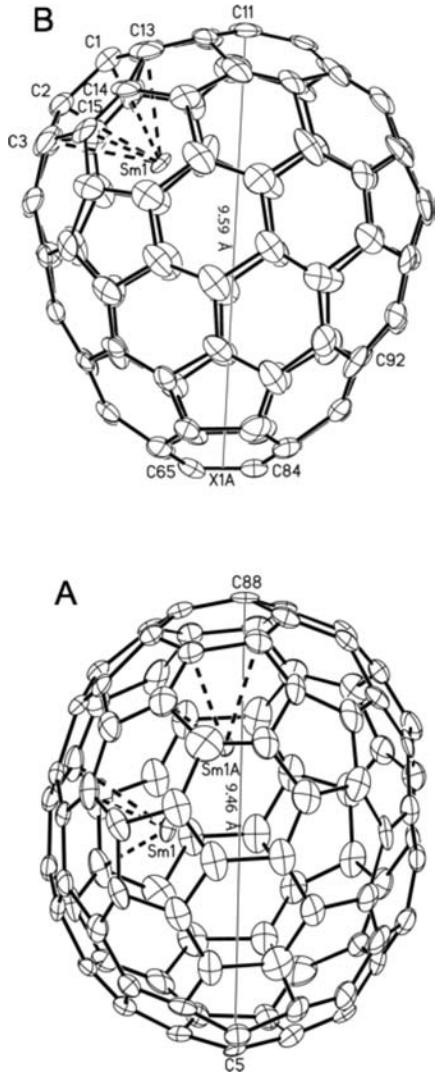

Figure 4. The structures of (A) Sm@C_1(42)-C_{92} in Sm@C_1(42)-C_{92}·Ni^{II}(OEP)·2(toluene) and (B) Sm@C_s(24)-C_{92} in Sm@C_s(24)-C_{92}·Ni^{II}(OEP)·1.6(toluene)·0.4(benzene). Thermal contours are shown at the 20% level in (A) and the 30% level in (B). The vertical line shows the long direction in each cage but is not a symmetry element. In (A) the major Sm site along with its symmetry generated counterpart is shown inside the predominant orientation of the cage. Only the major Sm site is shown in (B).

of the fullerene cage and two symmetry-related sites for the major samarium atom site. The crystallographic data indicate that Sm@C_{92}(I) utilizes a fullerene cage with no symmetry, C_1(42)-C_{92}, but one that does obey the IPR. This cage has a rather oblong shape with a long axis (as defined by the distance from C5 to C88) of 9.46 Å. The spatial relationship between the Ni(OEP) molecule and the endohedral fullerene can be seen by turning to Figure 5. As outlined in the Experimental Section, this structure suffers from disorder in the Sm positions.

dx.doi.org/10.1021/ja302859r | J. Am. Chem. Soc. 2012, 134, 10933–10941

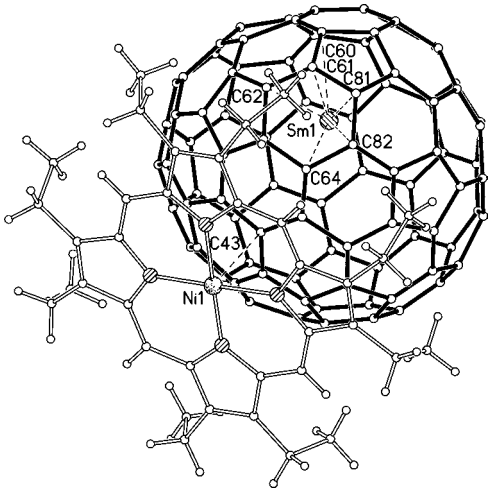

Figure 5. A drawing showing the orientation of the Ni^{II}(OEP) molecule with respect to the fullerene in Sm@C_1(42)-C_{92}·Ni^{II}(OEP)·2(toluene). The Ni···C43 distance is 2.983(4) Å. Only the major Sm site is shown.

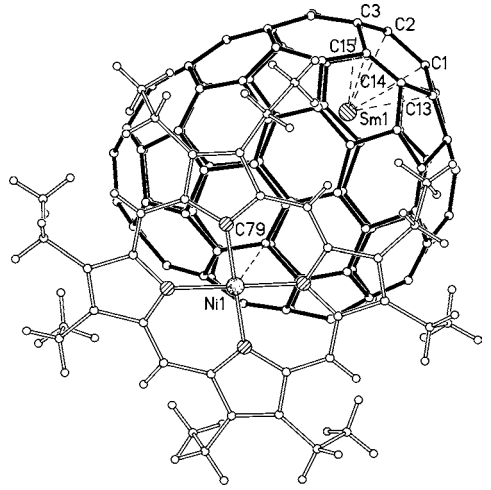

Figure 6. A drawing showing the orientation of the fullerene, Sm@C_1(42)-C_{92}, with respect to the Ni^{II}(OEP) molecule in Sm@C_s(24)-C_{92}·Ni^{II}(OEP)·1.6(toluene) ·0.4(benzene). The Ni···C79 distance is 3.053(6) Å. Only the major Sm site is shown.

The major samarium site has 50% occupancy, but there are four other samarium sites with occupancies ranging from 26% to 6%.

Crystallographic Identification of Sm@C_{92}(II) as Sm@C_s(24)-C_{92}. Cocrystallization of Sm@C_{92}(II) with Ni(OEP) produced crystals of Sm@C_s(24)-C_{92}·Ni^{II}(OEP)·1.6-(toluene)·0.4benzene, which were used for the crystallographic analysis. Figure 4B shows a drawing of Sm@C_s(24)-C_{92} that allows its structure to be compared to that of the other isomer. As with Sm@C_1(42)-C_{92}, the fullerene cage in Sm@C_{92}(II) obeys the IPR and has an oblong shape with an even longer distance of 9.59 Å between C11 at one apex and the midpoint of the C65−C84 bond at the opposite apex. There is more disorder in the Sm@C_s(24)-C_{92}·Ni^{II}(OEP)·1.6(toluene)·0.4-(benzene) structure than in the previous structure. For example, there are three C_{92} cages in the asymmetric unit with occupancies of 73%, 16%, and 11%, and there are seven Sm positions. The major position is at 50% occupancy, while the other six have occupancies ranging from 16% to 5%. Figure 6 shows the relative orientation of the major orientation of the fullerene and nickel porphyrin.

Computational Studies of the Sm@C_{92} Isomers. The electronic structures of samarium-containing endohedrals can be formally expressed as $Sm^{2+}@C_{2n}^{2-}$. Geometric optimizations using DFT methodology were conducted to compare Sm@C_1(42)-C_{92} and Sm@C_s(24)-C_{92}. The results are shown in Table 1. Sm@C_1(42)-C_{92}, which is the more abundant of the two isomers, is the more stable. It also possesses a smaller HOMO−LUMO gap than that of Sm@C_s(24)-C_{92}. In that regard, it is interesting to note that Sm@C_1(42)-C_{92} has a lower energy onset of absorption, at ca. 1330 nm, than Sm@C_s(24)-C_{92}, whose onset occurs at 1290 nm.

The electronic ground states of Sm@C_1(42)-C_{92} and Sm@C_s(24)-C_{92} possess a spin multiplicity of 7 due to the six 4f electrons on samarium. Using a Mulliken population analysis, the atomic charge on samarium in both isomers is 1.69. Thus, the net charge transferred from samarium to carbon cage is less than two.[57] According to a composition analysis of the orbitals, the samarium donates its two 6s electrons to the cage, but the 5d orbitals of samarium receive some back-donation of electrons from the occupied π orbitals of the cage. Consequently, there are weak covalent interactions between the samarium and the cage carbon atoms through the overlap of these orbitals. The occurrence of such back-donation has been suggested in another computational study on endohedrals of the type M@C_{82}.[57] The back-donation of the charge is consistent with the spin density distribution on the samarium, which slightly exceeds the maximum of 6, seen in Table 1. Figure 7 shows the computed spin distribution within the two Sm@C_{92} isomers with high spin density as expected on samarium and minor amounts of opposite spin transferred onto the immediately adjacent carbon atoms of the fullerene cage.

Figure 8 shows plots of the electrostatic potential in terms of total electron density mapped on the isosurface facing the Ni(OEP) molecule for the two isomers of Sm@C_{92}. The positions of the carbon atoms closest to the nickel atoms are indicated by red arrows and correspond to the closest contacts seen in Figures 5 and 6. As noted previously,[58] those positions on the fullerene surface nearest the nickel are in regions of significant positive potential as denoted by the blue-green color. This arrangement places regions of positive potential on the fullerene near regions of negative potential around the nitrogen atoms of the porphyrin as reported earlier for empty cage fullerenes such as D_{5h}(1)-C_{90}.[58]

Isolation of Four Isomers of Sm@C_{94}. Four isomers of Sm@C_{94} were isolated from the same carbon soot used to obtain the two Sm@C_{92} isomers. Details for the separation are given in the Supporting Information. The HPLC chromatograms of the purified samples of the four Sm@C_{94} isomers are shown in Figure 9. Of these, Sm@C_{94}(I) was the most abundant. The relative abundances of the four isomers were 100:20:25:1 for Sm@C_{94}(I), Sm@C_{94}(II), Sm@C_{94}(III), and Sm@C_{94}(IV), respectively. The much longer retention time of Sm@C_{94}(IV) suggests it has a much different shape than the other three isomers. Figure 10 shows the laser-desorption, time-of-flight (LD-TOF) mass spectrum of Sm@C_{94}(I) with the insets showing expansions of the experimental and computed spectra. The mass spectra for the other three isomers are similar and are given in the Supporting Information.

The UV−vis−NIR absorption spectra of the four Sm@C_{94} isomers are shown in Figure 11. The spectrum of Sm@C_{94}(I) shows an onset of absorption at 1230 nm and a series of

dx.doi.org/10.1021/ja302859r | J. Am. Chem. Soc. 2012, 134, 10933−10941

Table 1. Relative Energies (ΔE, kcal mol^{-1}) and HOMO−LUMO Gaps (in eV) of Sm@C_{92} and Sm@C_{94} Isomers Calculated at B3LYP/3-21g Level

isomer	ΔE, kcal mol^{-1}	HOMO−LUMO gap, eV	ground state	atomic charge on Sm	spin density on Sm
Sm@C_1(42)-C_{92}	0.0000	1.697	^{7}A	1.692	6.02
Sm@C_s(24)-C_{92}	0.3456	1.916	^{7}A″	1.689	6.03
Sm@C_{3v}(134)-C_{94}		2.159	^{7}A″	1.695	6.02

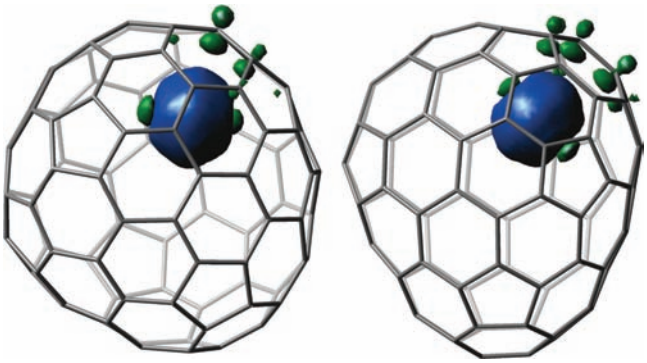

Figure 7. The spin density distributions of the Sm@C_1(42)-C_{92} (left) and Sm@C_s(24)-C_{92} (right) at the isovalue of 0.0005e.

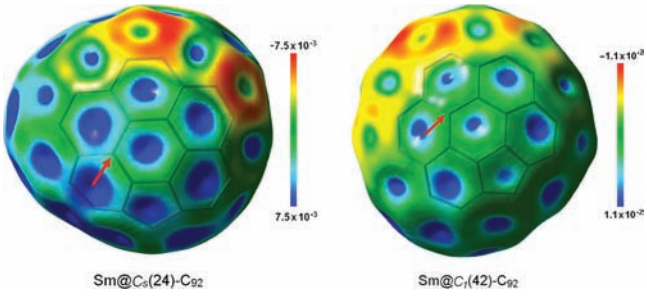

Figure 8. The plots of electrostatic potential in terms of total electron density (0.001 e/bohr^3) mapped on the isosurface facing the Ni(OEP) molecule for the two isomers of Sm@C_{92}. Two-dimensional projections of the bonds onto the plots are also shown for clarity. The red arrows indicate the carbon atoms nearest the nickel ion.

absorptions at 1137, 860, 780, 605, 475, and 436 nm. Earlier, Liu et al. reported that they had isolated three isomers of Sm@C_{94}.[25] The UV−vis−NIR spectrum they report for their isomer (I) is similar to the spectrum we report for Sm@C_{94}(I). Thus, both groups have produced the same isomer. However, the spectrum they show for their isomer II is rather similar to the spectrum they showed for their isomer I and, therefore, similar to our Sm@C_{94}(I). The spectrum reported for their isomer III is rather featureless, and we cannot associate it with any of the spectra shown in Figure 11. The UV−vis−NIR spectrum we report for Sm@C_{94}(I) is similar to the spectra reported for crystallographically characterized Ca@C_{3v}(134)-C_{94}[46] and Tm@C_{3v}(134)-C_{94}[46] and is also similar to that reported for Yb@C_{94}(I).[49]

Crystallographic Analysis of Sm@C_{94}(I) Reveals It Is Sm@C_{3v}(134)-C_{94}. Black parallelepipeds of Sm@C_{3v}(134)-C_{94}·Ni^{II}(OEP)·2toluene were obtained by cocrystallization of Sm@C_{94}(I) with Ni(OEP) and used for structural analysis. Attempts were made to obtain crystals from the other three isomers, but none of those efforts produced crystals that gave suitable X-ray diffraction. Figure 12 shows the structure of this endohedral, while Figure 13 shows the relative orientation of the fullerene and the Ni(OEP) molecule. In the major

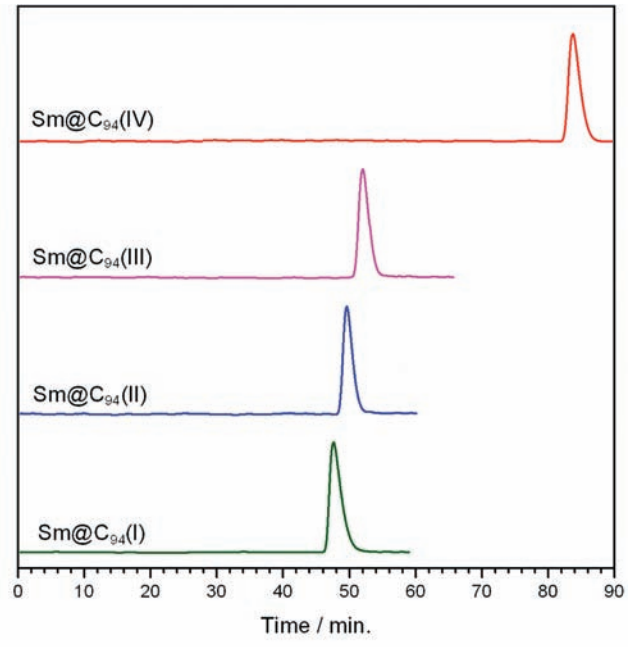

Figure 9. Chromatograms of the isolated Sm@C_{94} isomers on a Buckyprep column with toluene as the eluent. The HPLC conditions are flow rate 4.0 mL/min, detecting wavelength of 450 nm.

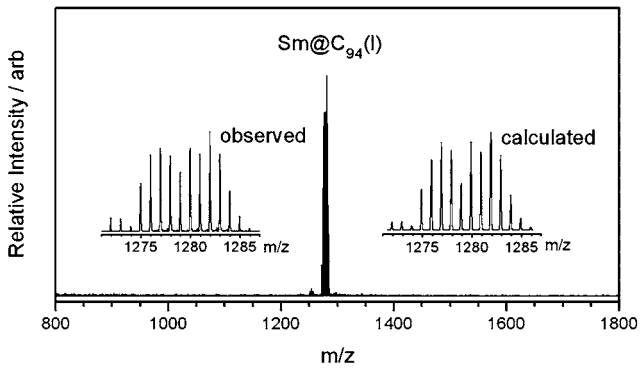

Figure 10. The LDI-TOF mass spectra of the purified sample of Sm@C_{94}(I). The insets show expansions of the observed and calculated isotope distributions. The experimental mass spectra of the other three isomers, which appear in the Supporting Information, are nearly identical and differ only in the signal-to-noise ratio in each spectrum.

orientation of the cage (83%), one of the mirror planes of the molecular C_{3v} symmetry coincides with a site of crystallographic mirror symmetry. The minor orientation (17% overall) does not utilize the crystallographic symmetry and is, therefore, disordered with respect to the mirror plane. The major Sm site (60.2%) and three minor Sm sites (21.2%, 13.2%, and 5.4%) are all located on the crystallographic mirror plane. In addition, Sm1 is located near the 3-fold axis of symmetry of the molecule and lies over one of the 6:6 ring

dx.doi.org/10.1021/ja302859r | J. Am. Chem. Soc. 2012, 134, 10933−10941

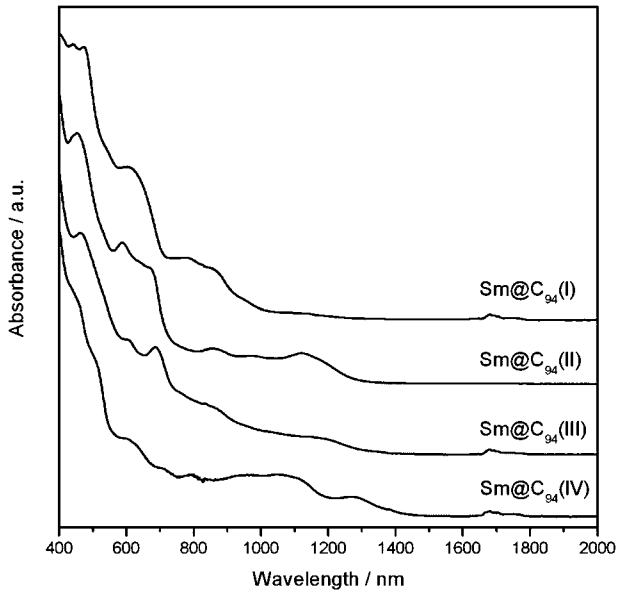

Figure 11. UV/vis/NIR absorption spectra of the purified isomers of Sm@C_{94} in carbon disulfide. The minor features in the 1650 − 1800 nm region are artifacts.

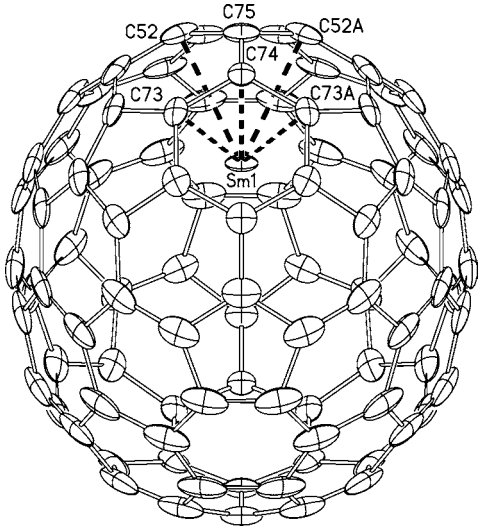

Figure 12. The structure of Sm@C_{3v}(134)-C_{94} in Sm@C_{3v}(134)-C_{94}·Ni^{II}(OEP)·2(toluene), showing the major form of the cage with 83% occupancy. Thermal contours are shown at the 35% probability level. The major Sm site with 60.2% occupancy is shown. There is a crystallographic mirror plane, which bisects C75, C74, and Sm1. All of the other three Sm sites line on this plane.

junctions that radiate from the C_3 axis. The two shortest Sm−C distances are 2.536(4) and 2.567(3) Å. The positioning of Sm1 in Sm@C_{3v}(134)-C_{94} is similar to that of the major calcium site in Ca@C_{3v}(134)-C_{94} and the major thulium site in Tm@C_{3v}(134)-C_{94}.[46] The length of the C_{94} cage as defined by the distance between C74, which lies at the apex of the 3-fold axis, and the centroid of the opposing hexagon is 9.007(7) Å.

Computational Studies on the Electronic Structure of Sm@C_{3v}(134)-C_{94}. Computational studies analogous to those performed for the Sm@C_{92} isomers were also conducted for Sm@C_{3v}(134)-C_{94}. Table 1 summarizes the relative energy, HOMO−LUMO gap, and spin density on Sm. Figure 14 shows the computed spin distribution within the Sm@C_{3v}(134)-C_{94}

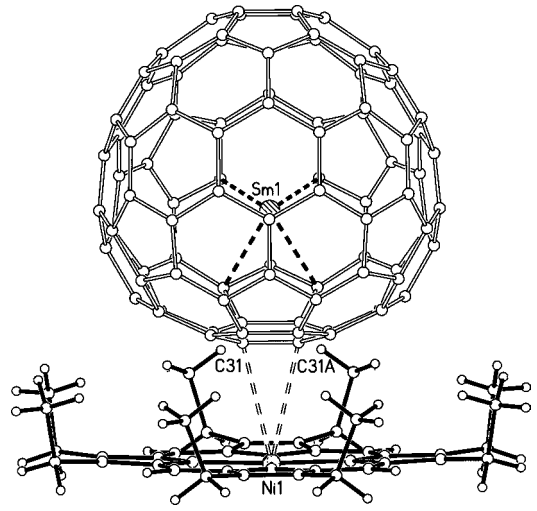

Figure 13. The orientation of Sm@C_{3v}(134)-C_{94} relative to the porphyrin in Sm@C_{3v}(134)-C_{94}·Ni^{II}(OEP)·2(toluene). The Ni···C31 distance is 3.161(3) Å. Only the major Sm site is shown.

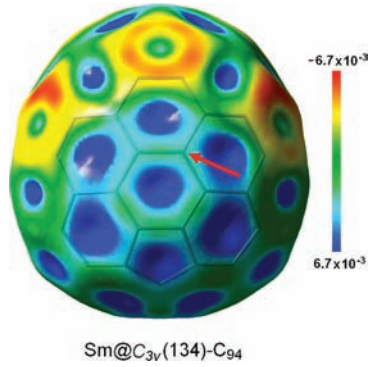

Figure 14. The plot of electrostatic potential in terms of total electron density (0.001 e/bohr^3) mapped on the isosurface facing the Ni(OEP) for Sm@C_{3v}(134)-C_{94}. Two-dimensional projection of the bonds onto the plot is also shown for clarity. The red arrow indicates the carbon atom nearest the nickel ion.

molecule. There is high spin density on the samarium ion and minor amounts of opposite spin transferred on the immediately adjacent six carbon atoms of the fullerene cage (Figure 15). Figure 8 shows plots of the electrostatic potential of Sm@C_{3v}(134)-C_{94} in terms of total electron density mapped on the isosurface facing the Ni(OEP) molecule. The positions of the

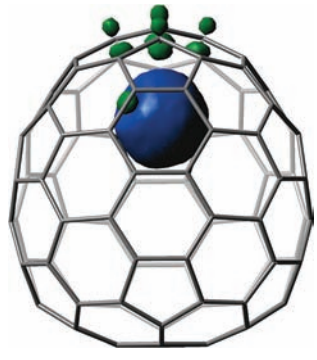

Figure 15. The spin density distributions of the Sm@C_{3v}(134)-C_{94} at the isovalue of 0.0005e.

dx.doi.org/10.1021/ja302859r | J. Am. Chem. Soc. 2012, 134, 10933−10941

Table 2. Crystal Data and Data Collection Parameters

	$Sm@C_1(42)$-C_{92} ·Ni^{II}(OEP)·2(toluene)	$Sm@C_s(24)$-C_{92} ·Ni^{II}(OEP)·1.6(toluene)·0.4(benzene)	$Sm@C_{3v}(134)$-C_{94} ·Ni^{II}(OEP)·2(toluene)
isomer	$Sm@C_{92}$(I)	$Sm@C_{92}$(II)	$Sm@C_{94}$(I)
formula	$C_{142}H_{60}N_4NiSm$	$C_{141.6}H_{59.2}N_4NiSm$	$C_{144}H_{60}N_4NiSm$
fw	2031.00	2025.39	2055.02
color, habit	black needle	black prism	black parallelepiped
crystal system	monoclinic	monoclinic	monoclinic
space group	*C*2/*m*	*C*2/*c*	*C*2/*m*
a, Å	25.5517(7)	47.306(4)	25.6869(8)
b, Å	15.3002(4)	15.0840(12)	15.1248(5)
c, Å	20.8629(6)	25.625(2)	21.3153(6)
β, deg	95.307(4)	117.664(2)	97.368(2)
V, Å^3	8121.3(4)	16195(2)	8212.8(4)
Z	4	8	4
T (K)	90(2)	90(2)	100(2)
radiation (*λ*, Å)	Mo K*α* 0.71073	Mo K*α* 0.71073	synchrotron 0.7749
unique data	12 776 [*R*(int) = 0.0369]	26 909 [*R*(int) = 0.0328]	16 962 [*R*(int) = 0.0647]
parameters	1196	6003	2683
restraints	1179	1622	1377
obsd ($I > 2\sigma(I)$) data	9384	18 786	16 962
R1[a] (obsd data)	0.0603	0.1203	0.0517
wR2[b] (all data)	0.1813	0.3520	0.1523

[a]For data with $I > 2\sigma I$, R1 = $(\sum||F_o| - |F_c||)/(\sum|F_o|)$. [b]For all data, wR2 = $(\sum[w(F_o^2 - F_c^2)^2])/(\sum[w(F_o^2)^2])^{1/2}$.

carbon atoms closest to the nickel atoms are indicated by red arrows and correspond to the contacts seen in Figure 13. As with the $Sm@C_{92}$ isomers, the portions of the fullerene surface nearest the nickel are regions of significant positive potential as denoted by the blue-green color.

DISCUSSION AND CONCLUSIONS

Two isomers of $Sm@C_{92}$ have been isolated and identified as $Sm@C_1(42)$-C_{92} and $Sm@C_s(24)$-C_{92}. Generally, fullerenes are highly symmetric. For example, consider the three most abundant fullerenes: C_{60} and $Sc_3N@I_h$-C_{80} have cages with icosahedral symmetry, while C_{70} has D_{5h} symmetry. However, as the sizes of the fullerene cages increase, the number of possible, IPR-obeying isomers with C_1 symmetry also increases. Thus, for C_{92}, 38 of the 86 IPR-obeying isomers have C_1 symmetry (while eight have C_s symmetry).[34] Recently, our laboratories reported the structural characterizations of the first pristine empty-cage fullerenes with C_1 symmetry, $C_1(30)$-C_{90} and $C_1(32)$-C_{90},[59] as well as the first endohedral fullerene with C_1 symmetry, $Sm_2@C_1(21)$-C_{90}.[43]

Unlike the situation for the four $Sm@C_{90}$ and the five $Sm@C_{84}$ isomers, where all isomers belong to common isomerization maps and can be converted into one another through Stone–Wales transformations as noted in the Introduction, $Sm@C_1(42)$-C_{92} and $Sm@C_s(24)$-C_{92} are not related to each other by any set of Stone–Wales transformations.[34] The fullerene cage $C_s(24)$-C_{92} cannot be converted into any other C_{92} isomer through Stone–Wales transformations, while $C_1(42)$-C_{92} belongs to an isomerization map that relates it to 57 other C_{92} isomers.[34] Thus, the formation of these endohedral fullerenes does not necessarily rely upon Stone–Wales transformations to produce the experimentally observed set of isomers. Similar considerations also pertain to empty cage fullerenes. For example, three isomers of C_{90} have been structurally characterized.[58,59] The most plentiful of these obtained from Sm_2O_3-doped graphite rods is $D_{5h}(1)$-C_{90}. This isomer cannot be converted into any other C_{90} isomer through Stone–Wales transformations.

It is significant to note that the fullerene isomers found in $Sm@C_1(42)$-C_{92} and $Sm@C_s(24)$-C_{92} are different from the isomer found in the related endohedral fullerenes containing a C_{92} cage, $Gd_2C_2@D_3(85)$-C_{92},[42] and $Sm_2@D_3(85)$-C_{92}.[43] As pointed out elsewhere, the charge transferred from the interior contents to the fullerene cage is a very significant factor in determining which cage isomer is most stable.[6,16,17] For $Sm_2@D_3(85)$-C_{92} and $Gd_2C_2@D_3(85)$-C_{92}, the cage accepts four electrons from the interior atoms, whereas in $Sm@C_1(42)$-C_{92} and $Sm@C_s(24)$-C_{92}, only two electrons are transferred from samarium to the carbon skeleton. The differences in charge transferred alter the selection of appropriate cage.

Four isomers of $Sm@C_{94}$ were isolated from carbon soot obtained by electric arc vaporization of carbon rods doped with Sm_2O_3. The most abundant of these isomers has been identified as $Sm@C_{3v}(134)$-C_{94}. For a carbon cage with 94 atoms, there are 134 isomers that obey the isolated pentagon rule, and 89 of these have C_1 symmetry. Only one isomer has C_{3v} symmetry, and this is the isomer that has been crystallographically characterized in the three $M^{2+}@C_{94}^{2-}$ species: $Sm@C_{3v}(134)$-C_{94}, $Ca@C_{3v}(134)$-C_{94}, and $Tm@C_{3v}(134)$-C_{94}.[55] It is interesting that this is not the most favorable isomer that would be expected based on the maximum pentagon isolation rule for a C_{94}^{2-} cage.[6] Yet, theoretical calculations for neutral $C_{3v}(134)$-C_{94} show that the HOMO, of e symmetry, can accommodate an additional two electrons to form the dianion (see the Supporting Information).

As seen with the isomers of $Sm@C_{90}$ and $Sm@C_{84}$,[28,31] there is considerable uncertainty on the locations of the samarium atoms in $Sm@C_1(42)$-C_{92}, $Sm@C_s(24)$-C_{92}, and $Sm@C_{3v}(134)$-C_{94} due to the presence of disorder in both the cages and the metal atom positions. It appears that the samarium atoms are rather free to move about the inside of these carbon cages and adopt a range of locations upon

dx.doi.org/10.1021/ja302859r | J. Am. Chem. Soc. 2012, 134, 10933–10941

crystallization. Drawings showing the locations of the major sites for the samarium ions relative to the fullerene cages are shown in the Supporting Information along with tables showing the shortest Sm−C distances.

EXPERIMENTAL SECTION

Formation and Isolation of the Sm@C_{92} and Sm@C_{94} Isomers. An 8 × 150 mm graphite rod filled with Sm_2O_3 and graphite powder (Sm:C atomic ratio 1:40) was vaporized as the anode in DC arc discharge under optimized conditions. The raw soot was sonicated in *o*-dichlorobenzene for 8 h and then filtered with aid of a vacuum. After the solvent was removed with a rotary evaporator, chlorobenzene was added to redissolve the dry extract. The resulting solution was subjected to a four-stage HPLC isolation process without recycling. Chromatographic details are given in the Supporting Information.

Ultraviolet−visible−near-infrared (UV−vis−NIR) spectra were obtained through the use of a UV-4100 spectrophotometer (Hitachi High-Technologies Corp.) with samples dissolved in carbon disulfide.

Crystal Growth. Black prisms of Sm@C_s(24)-C_{92}·Ni^{II}(OEP)·1.6(toluene)·0.4(benzene) were obtained by slow diffusion of a solution of Sm@C_{92}(I) in toluene into a solution of Ni^{II}(OEP) in benzene. Black needles of Sm@C_1(42)-C_{92}·Ni^{II}(OEP)·2(toluene) were obtained by the slow diffusion of a solution of Sm@C_{92}(I) in toluene into a solution of Ni^{II}(OEP) in toluene. Black parallelepipeds of Sm@C_{3v}(134)-C_{94}·Ni(OEP)·2toluene were obtained by diffusion of a solution of Sm@C_{94}(I) in toluene into a solution of Ni^{II}(OEP) in toluene.

Crystal Structure Determinations. The black crystals of both cocrystals were mounted in the nitrogen cold stream provided by a Cryo Industries low temperature apparatus on the goniometer head of a Bruker SMART diffractometer equipped with an ApexII CCD detector. Data were collected with the use of Mo Kα radiation (λ = 0.71073 Å). The crystal of Sm@C_{3v}(134)-C_{94}·Ni^{II}(OEP)·2(toluene) was mounted in the 100(2) K nitrogen cold stream provided by an Oxford Cryostream low temperature apparatus, on a Bruker diffractometer and detector of beamline 11.3.1 at the Advanced Light Source in Berkeley, CA. Diffraction data were collected using synchrotron radiation that was monochromated with silicon(111) to a wavelength of 0.77490(1) Å. Crystal data are given in Table 2. The structures were solved by direct methods (SHELXS97) and refined by full-matrix least-squares on F^2 (SHELXL97).[60]

The structure of Sm@C_1(42)-C_{92}·Ni^{II}(OEP)·2(toluene) shows disorder in the Sm sites. The final model included five Sm positions. Sm1 and Sm2 are the predominant sites, with occupancies of 0.25 and 0.13, respectively. Sm3, Sm4, and Sm5 were assigned occupancies of 0.05, 0.04, and 0.03, respectively. The total occupancy for all Sm's is 0.5 in the asymmetric unit, but, with Z = 4, there is one Sm per C_{92}. Only Sm1 and Sm2 were refined with anisotropic thermal parameters. One of the toluene sites is disordered with respect to a second orientation.

The structure of Sm@C_s(24)-C_{92}·Ni^{II}(OEP)·1.6(toluene)·0.4(benzene) shows disorder in some of its components. However, the major components of the structure, Sm1, the major orientation of C_{92}, and the Ni(OEP), are well-defined and easily show up from solution of the structure. The occupancy of Sm1 refined to near 0.50 and was, therefore, fixed at this value. The other six Sm positions have occupancies that range from 0.05 to 0.16 with the total occupancy of Sm in agreement with 1.00 Sm per C_{92}. There are three positions for the C_{92}; the major position, at a refined occupancy of 0.729(2), was freely refined with anisotropic displacement parameters. The other two orientations were found by successive difference maps and refinement of C_1(42)-C_{92} rigid groups based on the geometry of the major ball. The two minor orientations of C_1(42)-C_{92} were kept isotropic. Their refined occupancies are 0.160(2) and 0.111(2). The structure also contains two disordered solvate sites: one with two orientations of toluene with occupancies 0.65/0.35, and the other with toluene (0.60 occupancy) and two orientations of benzene (0.30 and 0.10 occupancy).

In crystals of Sm@C_{3v}(134)-C_{94}·Ni^{II}(OEP)·2toluene, there are two orientations of the C_{94} cage. The major orientation, with refined occupancy of 0.413(1), utilizes the crystallographic mirror symmetry. Thus, 8 atoms reside on the mirror plane and 43 are in general positions. The second orientation with 0.087(2) fractional occupancy does not use crystallographic symmetry, the ball is disordered with respect to the mirror plane, and the 94 carbon atoms were refined. There is also disorder involving four different Sm positions, all of which lie on a crystallographic mirror plane. Their refined occupancies, which were constrained to add to 0.5, are Sm1, 0.301(3), Sm2, 0.106(3), Sm3, 0.066(5), and Sm4, 0.027(6).

Computational Details. Geometries of Sm@C_1(42)-C_{92}, Sm@C_s(24)-C_{92}, and Sm@C_{3v}(134)-C_{94} were fully optimized by nonlocal density functional calculations at the B3LYP level.[61] The effective core potential and basis set developed by Stevens et al. were used for samarium (CEP-31g),[62] and the split-valence 3-21g basis set was used for carbon. All calculations were carried out with the Gaussian 03 program.[63]

ASSOCIATED CONTENT

Supporting Information

Isolation procedures, complete citation for ref 63, and computational results. X-ray crystallographic files in CIF format for Sm@C_1(42)-C_{92}·Ni^{II}(OEP)·2(toluene), Sm@C_s(24)-C_{92}·Ni^{II}(OEP)·1.6(toluene)·0.4(benzene), and Sm@C_{3v}(134)-C_{94}·Ni^{II}(OEP)·2toluene. This material is available free of charge via the Internet at http://pubs.acs.org.

AUTHOR INFORMATION

Corresponding Author

albalch@ucdavis.edu; hyang@cjlu.edu.cn; zyliu@zju.edu.cn; mmolmstead@ucdavis.edu

Notes

The authors declare no competing financial interest.

ACKNOWLEDGMENTS

We thank the U.S. National Science Foundation [Grant CHE-1011760 to A.L.B. and M.M.O.], the National Natural Science Foundation of China [11179039, 20971108], the National Basic Research Program of China [2011CB808200], and Zhejiang Provincial Natural Science Foundation of China [R12B010002], and the Advanced Light Source, Lawrence Berkeley Laboratory, for support. The Advanced Light Source is supported by the Director, Office of Science, Office of Basic Energy Sciences, of the U.S. Department of Energy under Contract No. DE-AC02-05CH11231.

REFERENCES

(1) Aldersey-Williams, H. *The Most Beautiful Molecule: The Discovery of the Buckyball*; Wiley: New York, 1997.

(2) Baggott, J. *Perfect Symmetry: The Accidental Discovery of Buckminsterfullerene*; Oxford University Press: Oxford, 1996.

(3) Heath, J. R.; O'Brien, S. C.; Zhang, Q.; Liu, Y.; Curl, R. F.; Kroto, H. W.; Tittel, F. K.; Smalley, R. E. *J. Am. Chem. Soc.* **1985**, *107*, 7779−7780.

(4) Akasaka, T., Wudl, F., Nagase, S., Eds. *Chemistry of Nanocarbons*; John Wiley & Sons, Ltd.: Singapore, 2010.

(5) Lu, X.; Akasaka, T.; Nagase, S. *Chem. Commun.* **2011**, *47*, 5942−5957.

(6) Rodríguez-Fortea, A.; Balch, A. L.; Poblet, J. M. *Chem. Soc. Rev.* **2011**, *40*, 3551−3563.

(7) Chaur, M. N.; Melin, F.; Ortiz, A. L.; Echegoyen, L. *Angew. Chem., Int. Ed.* **2009**, *48*, 7514−7538.

(8) Stevenson, S.; Rice, G.; Glass, T.; Harich, K.; Cromer, F.; Jordan, M. R.; Craft, J.; Hadju, E.; Bible, R.; Olmstead, M. M.; Maitra, K.; Fisher, A. J.; Balch, A. L.; Dorn, H. C. *Nature* **1999**, *401*, 55−57.

(9) Mercado, B. Q.; Jiang, A.; Yang, H.; Wang, Z.; Jin, H.; Liu, Z.; Olmstead, M. M.; Balch, A. L. *Angew. Chem., Int. Ed.* **2009**, *48*, 9114−9116.
(10) Murata, M.; Maeda, S.; Morinaka, Y.; Murata, Y.; Komatsu, K. *J. Am. Chem. Soc.* **2008**, *130*, 15800−15801.
(11) Mercado, B. Q.; Olmstead, M. M.; Beavers, C. M.; Easterling, M. L.; Stevenson, S.; Mackey, M. A.; Coumbe, C. E.; Phillips, J. D.; Phillips, J. P.; Poblet, J. M.; Balch, A. L. *Chem. Commun.* **2010**, *46*, 279−281.
(12) Saunders, M.; Cross, R. J.; Jimenez-Vazquez, H. A.; Shimshi, R.; Khong, A. *Science* **1996**, *271*, 1693−1697.
(13) Murphy, T. A.; Pawlik, T.; Weidinger., A; Hohne, M.; Alcala, R.; Spaeth, J. M. *Phys. Rev. Lett.* **1996**, *77*, 1075−1078.
(14) Knapp, C.; Dinse, K.-P.; Pietzak, B.; Waiblinger, M.; Weidinger, A. *Chem. Phys. Lett.* **1997**, *272*, 433−437.
(15) Mauser, H.; Hirsch, A.; van Eikema Hommes, N. J. R.; Clark, T.; Pietzak, B.; Weidinger, A.; Dunsch, L. *Angew. Chem., Int. Ed. Engl.* **1997**, *36*, 2835−2838.
(16) Rodríguez-Fortea, A.; Balch, A. L.; Poblet, J. M. *Chem. Soc. Rev.* **2011**, *40*, 3551−3563.
(17) Rodriguez-Fortea, A.; Alegret, N.; Balch, A. L.; Poblet, J. M. *Nat. Chem.* **2010**, *2*, 955−961.
(18) Alegret, N.; Mulet-Gas, M.; Aparicio-Anglès, X.; Rodríguez-Fortea, A.; Poblet, J. M. *C. R. Chimie* **2012**, *15*, 152−158.
(19) Shultz, M. D.; Duchamp, J. C.; Wilson, J. D.; Shu, C.-Y.; Ge, J.; Zhang, J.; Gibson, H. W.; Fillmore, H. L.; Hirsch, J. I.; Dorn, H. C.; Fatouros, P. P. *J. Am. Chem. Soc.* **2010**, *132*, 4980−4981.
(20) Shultz, M. D.; Wilson, J. D.; Fuller, C. E.; Zhang, J.; Dorn, H. C.; Fatouros, P. P. *Radiology* **2011**, *261*, 136−143.
(21) Mikawa, M.; Kato, H.; Okumura, M.; Narazaki, M.; Kanazawa, Y.; Miwa, N.; Shinohara, H. *Bioconjugate Chem.* **2001**, *12*, 510−514.
(22) Bolskar, R. D.; Benedetto, A. F.; Husebo, L. O.; Price, R. E.; Jackson, E. F.; Wallace, S.; Wilson, L. J.; Alford, J. M. *J. Am. Chem. Soc.* **2003**, *125*, 5471−5478.
(23) Okazaki, T.; Lian, Y.; Gu, Z.; Suenaga, K.; Shinohara, H. *Chem. Phys. Lett.* **2000**, *320*, 435−440.
(24) Lian, Y.; Shi, Z.; Zhou, X.; He, X.; Gu, Z. *Chem. Mater.* **2001**, *13*, 39−42.
(25) Liu, J.; Shi, Z.; Gu, Z. *Chem. Asian J.* **2009**, *4*, 1703−1711.
(26) Okazaki, T.; Suenaga, K.; Lian, Y.; Gu, Z.; Shinohara, H. *J. Chem. Phys.* **2000**, *113*, 9593−9597.
(27) Okazaki, T.; Suenaga, K.; Lian, Y.; Gu, Z.; Shinohara, H. *J. Mol. Graphics Modell.* **2001**, *19*, 244−251.
(28) Yang, H.; Jin, H. X.; Zhen, H.; Wang, Z. M.; Liu, Z. L.; Beavers, C. M.; Mercado, B. Q.; Olmstead, M. M.; Balch, A. L. *J. Am. Chem. Soc.* **2011**, *133*, 6299−6306.
(29) Stone, A. J.; Wales, D. J. *Chem. Phys. Lett.* **1986**, *128*, 501−503.
(30) Cross, R. J.; Saunders, M. *J. Am. Chem. Soc.* **2005**, *127*, 3044−3047.
(31) Yang, H.; Yu, M.; Jin, H.; Liu, Z.; Yao, M.; Liu, B.; Olmstead, M. M.; Balch, A. L. *J. Am. Chem. Soc.* **2012**, *134*, 5331−5338.
(32) (a) Okazaki, T.; Lian, Y. F.; Gu, Z. N.; Suenaga, K.; Shinohara, H. *Chem. Phys. Lett.* **2000**, *320*, 435−440. (b) Lian, Y.; Shi, Z.; Zhou, X.; He, X.; Gu, Z. *Chem. Mater.* **2001**, *13*, 39−42.
(33) Lu, X.; Slanina, Z.; Akasaka, T.; Tsuchiya, T.; Mizorogi, N.; Nagase, S. *J. Am. Chem. Soc.* **2010**, *132*, 5896−5905.
(34) Fowler, P. W.; Manolopoulos, D. E. *An Atlas of Fullerenes*; Clarendon: Oxford, 1995.
(35) Wakahara, T.; Nikawa, H.; Kikuchi, T.; Nakahodo, T.; Rahman, G. M. A.; Tsuchiya, T.; Maeda, Y.; Akasaka, T.; Yoza, K.; Horn, E.; Yamamoto, K.; Mizorogi, N.; Slanina, Z.; Nagase, S. *J. Am. Chem. Soc.* **2006**, *128*, 14228−14229.
(36) Wang, C.-R.; Kai, T.; Tomiyama, T.; Yoshida, T.; Kobayashi, Y.; Nishibori, E.; Takata, M.; Sakata, M.; Shinohara, H. *Nature* **2000**, *408*, 426−427.
(37) Olmstead, M. M.; Lee, H. M.; Duchamp, J. C.; Stevenson, S.; Marciu, D.; Dorn, H. C.; Balch, A. L. *Angew. Chem., Int. Ed.* **2003**, *42*, 900−903.
(38) Lu, X.; Nikawa, H.; Nakahodo, T.; Tsuchiya, T.; Ishitsuka, M. O.; Maeda, Y.; Akasaka, T.; Toki, M.; Sawa, H.; Slanina, Z.; Mizorogi, N.; Nagase, S. *J. Am. Chem. Soc.* **2008**, *130*, 9129−9136.
(39) Beavers, C. M.; Zuo, T.; Duchamp, J. C.; Harich, K.; Dorn, H. C.; Olmstead, M. M.; Balch, A. L. *J. Am. Chem. Soc.* **2006**, *128*, 11352−11353.
(40) Mercado, B. Q.; Beavers, C. M.; Olmstead, M. M.; Chaur, M. N.; Walker, K.; Holloway, B. C.; Echegoyen, L.; Balch, A. L. *J. Am. Chem. Soc.* **2008**, *130*, 7854−7855.
(41) Beavers, C. M.; Chaur, M. N.; Olmstead, M. M.; Echegoyen, L.; Balch, A. L. *J. Am. Chem. Soc.* **2009**, *131*, 11519−11524.
(42) Yang, H.; Lu, C.; Liu, Z.; Jin, H.; Che, Y.; Olmstead, M. M.; Balch, A. L. *J. Am. Chem. Soc.* **2008**, *130*, 17296−17300.
(43) Yang, H.; Jin, H.; Hong, B.; Liu, Z.; Beavers, C. M.; Zhen, H.; Wang, Z.; Mercado, B. Q.; Olmstead, M. M.; Balch, A. L. *J. Am. Chem. Soc.* **2011**, *133*, 16911−16919.
(44) Troyanov, S. I.; Tamm, N. B. *Chem. Commun.* **2009**, 6035−6037.
(45) Lamm, N. B.; Sidorov, L. N.; Kemnitz, E.; Troyanov, S. I. *Angew. Chem., Int. Ed.* **2009**, *48*, 9102−9104.
(46) Che, Y.; Yang, H.; Wang, Z.; Jin, H.; Liu, Z.; Lu, C.; Zuo, T.; Dorn, H.; Beavers, C. M.; Olmstead, M. M.; Balch, A. L. *Inorg. Chem.* **2009**, *48*, 6004−6010.
(47) Sun, D.-Y.; Liu, Z.-Y.; Guo, X.-H.; Xu, W.-G.; Liu, S.-Y. *J. Phys. Chem. B* **1997**, *101*, 3927−3930.
(48) Xu, J. X.; Wang, Z. Y.; Shi, Z. J.; Gu, Z. N. *Chem. Phys. Lett.* **2005**, *409*, 192−196.
(49) Che, Y. L.; Yang, H.; Jin, H. X.; Lu, C. X.; Liu, Z. Y. *J. Chem. Sci.* **2009**, *121*, 297−300.
(50) Tagmatarchis, N.; Shinohara, H. *Chem. Mater.* **2000**, *12*, 3222−3226.
(51) Tagmatarchis, N.; Aslanis, E.; Prassides, K.; Shinohara, H. *Chem. Mater.* **2001**, *13*, 2374−2379.
(52) Xenogiannopoulou, E.; Couris, S.; Koudoumas, E.; Tagmatarchis, N.; Inoue, T.; Shinohara, H. *Chem. Phys. Lett.* **2004**, *394*, 14−18.
(53) Chaur, M. N.; Melin, F.; Ashby, J.; Elliott, B.; Kumbhar, A.; Rao, A. M.; Echegoyen, L. *Chem.-Eur. J.* **2008**, *14*, 8213−8219.
(54) Xu, J. X.; Wang, Z. Y.; Shi, Z. J.; Gu, Z. N. *Chem. Phys. Lett.* **2005**, *409*, 192−196.
(55) Richter, H.; Labrocca, A. J.; Grieco, W. J.; Taghizadeh, K.; Lafleur, A. L.; Howard, J. B. *J. Phys. Chem. B* **1997**, *101*, 1556−1560.
(56) Olmstead, M. M.; Costa, D. A.; Maitra, K.; Noll, B. C.; Phillips, S. L.; Van Calcar, P. M.; Balch, A. L. *J. Am. Chem. Soc.* **1999**, *121*, 7090−7097.
(57) Kobayashi, K.; Nagase, S. *Chem. Phys. Lett.* **1998**, *282*, 325−329.
(58) Yang, H.; Beavers, C. M.; Wang, Z.; Jiang, A.; Liu, Z.; Jin, H.; Mercado, B. Q.; Olmstead, M. M.; Balch, A. L. *Angew. Chem., Int. Ed.* **2010**, *49*, 886−890.
(59) Yang, H.; Mercado, B. Q.; Jin, H.; Wang, Z.; Jiang, A.; Liu, Z.; Beavers, C.; Olmstead, M. M.; Balch, A. L. *Chem. Commun.* **2011**, *47*, 2068−2070.
(60) Sheldrick, G. M. *Acta Crystallogr.* **2008**, *A64*, 112−122.
(61) (a) Becke, A. D. *Phys. Rev. A* **1988**, *38*, 3098−3100. (b) Lee, C.; Yang, W.; Parr, R. G. *Phys. Rev. B* **1988**, *37*, 785−789.
(62) Stevens, W.; Basch, H.; Krauss, J. *J. Chem. Phys.* **1984**, *81*, 6026−6033.
(63) Frisch, M. J.; et al. *Gaussian 03*, revision C.02; Gaussian, Inc.: Wallingford, CT, 2004.